universe

MDPI

Communication

Gamma-Ray Bursts Calibrated by Using Artificial Neural Networks from the Pantheon+ Sample

Zhen Huang [1,†], Xin Luo [1,†], Bin Zhang [2], Jianchao Feng [3], Puxun Wu [4], Yu Liu [5] and Nan Liang [1,*]

[1] Guizhou Key Laboratory of Advanced Computing, Guizhou Normal University, Guiyang 550025, China; zhen_huang@gznu.edu.cn (Z.H.); xin_luo@gznu.edu.cn (X.L.)
[2] School of Mathematical Sciences, Guizhou Normal University, Guiyang 550025, China; binzhang@gznu.edu.cn
[3] Department of Astronomy, Guizhou Normal University, Guiyang 550025, China; fengjc@gznu.edu.cn
[4] Department of Physics and Synergistic Innovation Center for Quantum Effects and Applications, Hunan Normal University, Changsha 410081, China; pxwu@hunnu.edu.cn
[5] School of Physical Science and Technology, Southwest Jiaotong University, Chengdu 611756, China; lyu@swjtu.edu.cn
* Correspondence: liangn@bnu.edu.cn
† These authors contributed equally to this work.

Abstract: In this paper, we calibrate the luminosity relation of gamma−ray bursts (GRBs) by employing artificial neural networks (ANNs) to analyze the Pantheon+ sample of type Ia supernovae (SNe Ia) in a manner independent of cosmological assumptions. The A219 GRB dataset is used to calibrate the Amati relation ($E_{\rm p}$-$E_{\rm iso}$) at low redshift with the ANN framework, facilitating the construction of the Hubble diagram at higher redshifts. Cosmological models are constrained with GRBs at high redshift and the latest observational Hubble data (OHD) via the Markov chain Monte Carlo numerical approach. For the Chevallier−Polarski−Linder (CPL) model within a flat universe, we obtain $\Omega_{\rm m} = 0.321^{+0.078}_{-0.069}$, $h = 0.654^{+0.053}_{-0.071}$, $w_0 = -1.02^{+0.67}_{-0.50}$, and $w_a = -0.98^{+0.58}_{-0.58}$ at the $1-\sigma$ zconfidence level, which indicates a preference for dark energy with potential redshift evolution ($w_a \neq 0$). These findings using ANNs align closely with those derived from GRBs calibrated using Gaussian processes (GPs).

Keywords: gamma-ray bursts; general cosmology; dark energy cosmology; observations

Academic Editor: Firstname Lastname

Received: 11 June 2025
Revised: 15 July 2025
Accepted: 17 July 2025
Published:

Citation: Huang, Z.; Luo, X.; Zhang, B.; Feng, J.; Wu, P.; Liu, Y.; Liang, N. Gamma-Ray Bursts Calibrated by Using Artificial Neural Networks from the Pantheon+ Sample. *Universe* **2025**, *1*, 0. https://doi.org/

1. Introduction

Gamma−ray bursts (GRBs) can serve as cosmic probes by leveraging luminosity relations to explore the universe's expansion history at redshifts far beyond Type Ia supernovae (SNe Ia) [1–9]. To address the circularity problem, Ref. [10] proposed a model−independent method to calibrate seven GRB luminosity relations utilizing SNe Ia at low redshifts. In [11], the authors used observational Hubble data (OHD) obtained via the cosmic chronometers (CC) method to calibrate the Amati relation, which connects the spectral peak energy to the isotropic equivalent radiated energy [12]. Therefore, GRB data can be used to constrain cosmological models at high redshift by using the standard Hubble diagram method [13–23]. Other local data have also been used to calibrate GRBs, e.g., mock data of gravitational waves (GWs) [24], quasars [25,26], and angular diameter distances of galaxy clusters [27]. In addition,Ref. [28] proposed the simultaneous fitting method, which constrains the coefficients of the relationship and the parameters of the cosmological model simultaneously to alleviate the circularity problem. It has been found that the Amati relation parameters are almost identical in all cosmological models by the simultaneous fitting method with a

dataset of 118 GRBs (the A118 sample) from the total 220 GRBs (the A220 sample) [29–33]. Recent works on the luminosity relations of GRBs and their applications for cosmology can be found in [34–42]; see [43,44] for reviews.

Similar to the interpolation method used in [10] and the Bézier parametric used in [11], GRBs can be calibrated from local data using iterative procedures [45], polynomial fitting [46], local regression [15,47], cosmography methods [48,49], the Padé approximation method [50], or a two−step method [51,52]. Recently, Gaussian processes (GPs) [53] have been used in GRB cosmological studies [54–61]. However, in GP analysis it is typically assumed that the errors in observational data follow a Gaussian distribution [53], which may pose a substantial limitation when reconstructing functions from data; furthermore, the results can be affected by the choice of the kernel functions, with many different available kernel functions [62,63]. The application of machine learning (ML) techniques has revolutionized data analysis in cosmology, offering robust tools for reconstructing complex astrophysical relationships and constraining cosmological parameters. In [64], the authors explored three ML treatments (linear regression, neural network, random forest) to alleviate the circularity problem with the Amati relation. In [65], machine learning algorithms were deployed to measure H_0 through regression analysis, finding that Support Vector Machine (SVM) exhibited the best performance in terms of bias−variance tradeoff in most cases, showing itself to be a competitive cross−check to GP. In [66], the authors utilized high−performance KNN (K-Nearest Neighbors) and RF (Random Forest) machine learning algorithms based on the Pantheon+ dataset [67] and the A219 sample [32,55] to calibrate the Amati relation in a model−independent manner and construct the Hubble diagram. By combining high−redshift data and observational Hubble data to constrain cosmological models, their results are consistent with those calibrated by Gaussian processes, providing a new pathway for precise cosmological studies.

Moreover, ANNs excel in modeling nonlinear correlations without requiring predefined functional forms, which can be used for cosmology at high redshifts [68–75]. In the context of GRBs, ANN−based approaches can provide a powerful framework for calibrating empirical luminosity relations. In [76], the authors used a novel deep learning framework to reconstruct the cosmic distance ladder with a GRB sample, while [77] employed neural networks to calibrate the Dainotti relations[1] from the Pantheon+ sample of SNe Ia. In [80], an ANN framework was employed based on observational Hubble data (OHD) from cosmic chronometers, reconstructing $H(z)$ in a model−independent way for relation calibration. Considering the physical correlations in the data, the authors introduced the covariance matrix and Kullback−Leibler (KL) divergence into the loss function, then used the A219 [32,55] and J220 samples [81,82] to select the optimal ANN model for calibrating the Amati relation.

Recent advances have incorporated machine learning approaches such as ANNs in combination with Bayesian neural networks (BNNs) to enhance the precision and reliability of these calibrations while quantifying uncertainties in a cosmology−independent manner [83–85]. In this study, we employ a hybrid ANN+BNN framework to calibrate the Amati relation. We utilize the Pantheon+ sample of SNe Ia to construct a high−redshift Hubble diagram and derive constraints on cosmological parameters in a flat universe, offering insights into the evolution of dark energy.

2. Reconstructing the Apparent Magnitude Redshift Relation from Pantheon+ Data

We explore the apparent magnitude−redshift relation using a hybrid model that integrates artificial (ANN) and Bayesian (BNN) neural networks. The ANN component models the relationship between redshift and apparent magnitude, while the BNN quanti-

fies predictive uncertainties, accounting for the covariance errors inherent in the SNe Ia observations. Through backpropagation [86], the network iteratively refines its weights to minimize the loss function, [2] ensuring robust predictions. While ANNs excel in capturing complex patterns, they lack inherent uncertainty quantification. To address this, we employ a BNN approach, utilizing dropout to approximate Bayesian inference [87,88]. The ANN with dropout is run for 1000 iterations, producing a distribution of predicted magnitudes $m^j(z_i)$ for each redshift. The mean of these predictions serves as the final $m(z_i)$, with the standard deviation providing the uncertainty $\sigma_{m(z_i)}$. The ANN processes redshift inputs z_i to generate corresponding apparent magnitudes $m(z_i)$, as illustrated in Figure 1.

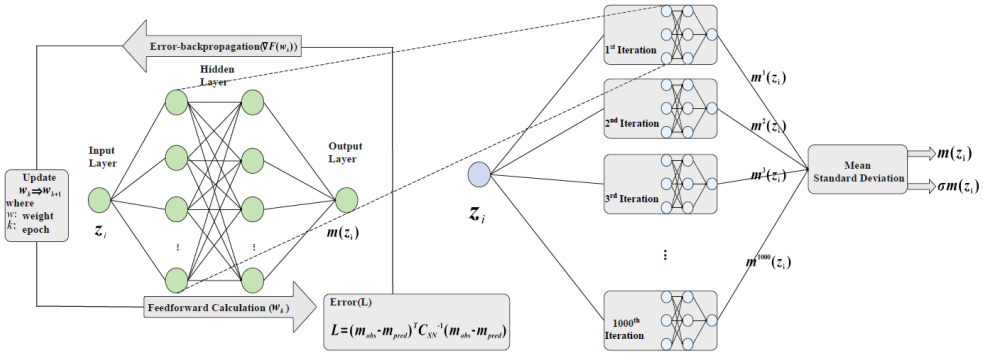

Figure 1. Architecture of the ANN+BNN framework for fitting Pantheon+ SNe Ia apparent magnitudes $m(z_i)$. The left panel depicts the ANN structure, which maps the redshift z_i to $m(z_i)$. The right panel shows the BNN simulation, where the ANN with dropout is executed over 1000 iterations for a given z_i. The mean of these predictions provides $m(z_i)$, while the standard deviation yields the uncertainty $\sigma_{m(z_i)}$.

Effective model performance depends on well−tuned hyperparameters, including the batch size, number and structure of hidden layers, activation function, and dropout rate, which together mitigate overfitting and enhance generalization ability [89]. We performed a grid search across 360 combinations, as summarized in Table 1, selecting the configuration with the lowest loss. This configuration consisted of a batch size of 16, one hidden layer with 512 units, a Tanh activation function, and a dropout rate of 0.1.

Table 1. Candidate hyperparameters for the ANN+BNN framework used to model Pantheon+ SNe Ia apparent magnitudes $m(z_i)$. Optimal values determined via grid search are highlighted in bold.

Hyperparameter		**Candidate Values**
Batch size		**16**, 32, 64
Hidden layers	Layers	Units
	1	64, 128, 256, **512**
	2	(64, 32), (128, 64)
	3	(256, 128, 64), (512, 256, 128)
Activate function		ReLU, Sigmoid, **Tanh**
Dropout rate		**0.1**, 0.2, 0.3, 0.4, 0.5

The ANN+BNN reconstruction for fitting Pantheon+ SNe Ia apparent magnitudes $m(z_i)$ are shown in Figure 2. In this work, we utilize the A219 sample [55],[3] which is divided into a low−redshift subset ($z < 1.4$, 79 GRBs) for calibration and a high-redshift subset ($z \geq 1.4$, 182 GRBs) for cosmological analysis.

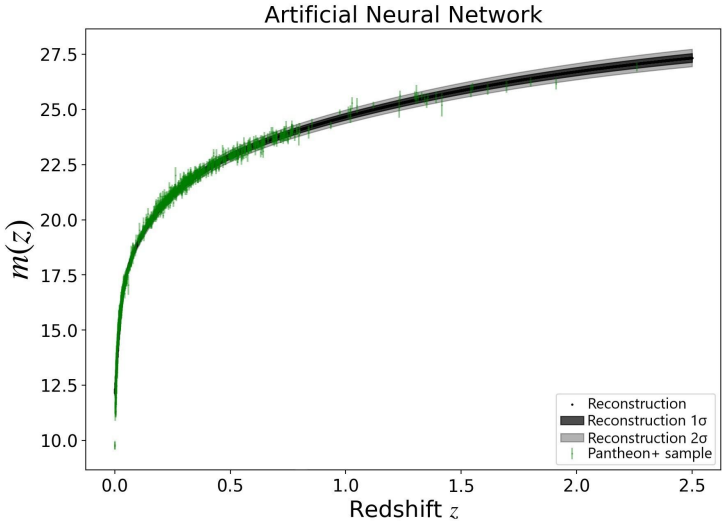

Figure 2. Reconstruction of the relation between the apparent magnitude and the redshift from the Pantheon+ dataset using the proposed ANN+BNN. Green dots indicate Pantheon+ data points with 1σ error bars. The black line represents the reconstructed central value, with shaded regions denoting 1σ and 2σ uncertainties.

3. Calibration of Amati Relation

The Amati relation linking the spectral peak energy ($E_{\rm p}$) to the isotropic equivalent radiated energy ($E_{\rm iso}$) is formulated as follows:

$$y = a + bx \tag{1}$$

where $y = \log_{10}\frac{E_{\rm iso}}{1\,{\rm erg}}$, $x = \log_{10}\frac{E_{\rm p}}{300\,{\rm keV}}$, and a and b are free parameters. These quantities are defined as $E_{\rm iso} = 4\pi d_L^2(z) S_{\rm bolo}(1+z)^{-1}$, $\quad E_{\rm p} = E_{\rm p}^{\rm obs}(1+z)$, with $d_L(z)$ as the luminosity distance, $S_{\rm bolo}$ as the bolometric fluence, and $E_{\rm p}^{\rm obs}$ as the observed spectral peak energy. The apparent magnitude m can be used to calibrate the relations between X−ray luminosity (L_X) and ultraviolet luminosity (L_{UV}) of quasars without assuming a prior absolute magnitude of SNe Ia[4] by introducing a new coefficient β' as a free parameter [90]. Furthermore, the Amati relation can be reformulated in terms of apparent magnitude m and a new coefficient a' as a free parameter [66]: $y' = a' + bx$, where $y' = \log_{10}\left[(1+z)^{-1}\left(\frac{S_{\rm bolo}}{1\,{\rm erg\,cm^{-2}}}\right)\right] + \frac{2}{5}m$ and $a' = a + 2\left(\frac{M}{5} - 1\right) - \log_{10}[4\pi({\rm pc/cm})^2]$. This permits calibration directly from observed GRB data using the apparent magnitude of SN Ia reconstructed at a redshift of GRBs at the same redshift.

We implement Markov chain Monte Carlo (MCMC) fitting via the emcee package [91]. Parameters are fitted using the likelihood method of [92],[5] which can avoid bias in variable selection [93,94]. We also used the GP method for comparison, which was done via the GaPP package with a squared exponential covariance function [53]. Results for the low-redshift A219 sample ($z < 1.4$) are presented in Table 2. We find that the ANN+BNN results align with those obtained by GP with the A219 sample ($z < 0.8$) [56] at 1σ uncertainties, confirming the efficacy of machine learning approaches. We also find that the quality of the uncertainty estimates produced here are not well−calibrated; the value of the intrinsic scatter obtained by our method in this case is slightly larger than other values obtained in the literature. It should be noted that the KL divergence, which considers the physical meaning represented by the reconstruction data with their uncertainties and the covariance matrix of data, should be introduced into the loss function in order to correct potential miscalibrations [80]. Actually, given the critical role of uncertainty quantification

in astrophysical inference, ensuring that ANNs produce reliable calibrated uncertainties is essential for their robust application in cosmology.

Table 2. Best−fitting parameters (a', b, $\sigma_{\rm int}$) for the Amati relation in the A219 GRB sample at $z < 1.4$ (79 GRBs) by ANN and GaPP methods along with the likelihood [92].

Methods	Datasets	a'	b	$\sigma_{\rm int}$
ANN	79 GRBs ($z < 1.4$)	$4.89^{+0.05}_{-0.05}$	$1.99^{+0.12}_{-0.15}$	0.55
GaPP	79 GRBs ($z < 1.4$)	$4.88^{+0.07}_{-0.07}$	$2.25^{+0.16}_{-0.21}$	0.71

4. The GRB Hubble Diagram and Constraints on DE Models

Assuming that the low−redshift calibration extends to higher redshifts, we construct the GRB Hubble diagram for $z \geq 1.4$. While the redshift dependence of GRB relations remains debated [15,25,32,39,40,82,84,95–98], we apply the calibrated Amati relation, noting that evolutionary effects warrant further scrutiny. By extrapolating the calibrated from the low−redshift GRBs to the high−redshift results using the ANN+BNN, we can obtain GRB Hubble diagram. The diagram combines low−redshift ($z < 1.4$) and high−redshift ($z \geq 1.4$) GRBs is shown in Figure 3.[6] To investigate dark energy (DE) properties, we leverage the high−redshift GRB Hubble diagram from the A219 sample to constrain the cosmological parameters in various DE models. We consider two flat models: the ΛCDM model with a constant equation of state (EoS) $w = -1$, and the Chevallier−Polarski−Linder (CPL) model [99,100] with a redshift−dependent EoS: $w(z) = w_0 + w_a z/(1+z)$.[7]

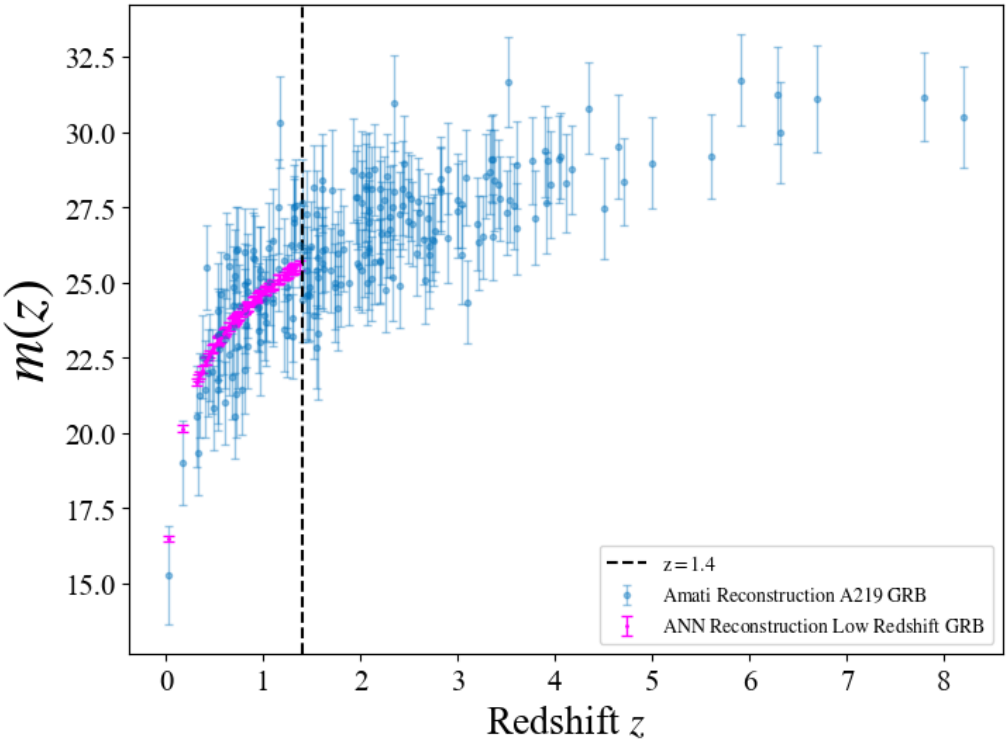

Figure 3. GRB Hubble diagram for the A219 dataset. Purple points denote GRBs at $z < 1.4$ derived from Pantheon+ using the proposed ANN+BNN. Blue points denote GRBs with the Amati relation calibrated using the likelihood method [92], including low−redshift ($z < 1.4$) and high−redshift ($z \geq 1.4$) GRBs.

We fit the cosmological parameters by minimizing the χ^2 statistic, incorporating the GRB covariance matrix $C_{\rm GRB}$. The χ^2 function for GRBs is defined as follows:

$$\chi^2_{\rm GRB} = \Delta m^T_{\rm GRB} C^{-1}_{\rm GRB} \Delta m_{\rm GRB} \tag{2}$$

where $\Delta m_{\rm GRB} = m_{\rm GRB} - m_{\rm th}(P)$ is the residual vector between observed apparent magnitudes $m_{\rm GRB}$ and theoretical magnitudes $m_{\rm th}(P)$, and is calculated for cosmological parameters P. The theoretical magnitude is provided by

$$m_{\rm th}(P) = 5\log_{10}\frac{d_L(P)}{\rm Mpc} + 25 + M = 5\log_{10} D_L(P) - \mu_0 + M, \tag{3}$$

where $D_L(P) = d_L(P)H_0$ is the unanchored luminosity distance, $\mu_0 = 5\log_{10} h + 42.38$, $h = H_0/(100\,{\rm km/s/Mpc})$, and H_0 is the Hubble constant.

To enhance constraints, we incorporate 32 OHD measurements, including 31 Hubble parameter data points at $0.07 < z < 1.965$ [101–106] and one additional point at $z = 0.80$ [107].[8] The OHD χ^2 is

$$\chi^2_{\rm OHD} = \Delta\hat{H}^T \mathbf{C}_H^{-1} \Delta\hat{H} + \chi^2_{\rm uncor}, \tag{4}$$

where $\Delta\hat{H} = H_{\rm th}(z;p) - H_{\rm obs}(z)$ for 15 correlated measurements [101–103], C_H^{-1} is the inverse covariance matrix [109], and $\chi^2_{\rm uncor} = \sum_{i=1}^{17}[H_{\rm th}(z_i;p) - H_{\rm obs}(z_i)]^2/\sigma^2_{H,i}$ for 17 uncorrelated measurements. The theoretical Hubble parameter is $H_{\rm th}(z;p) = H_0\sqrt{\Omega_{\rm m}(1+z)^3 + \Omega_{\rm DE}X(z)}$. The total χ^2 is

$$\chi^2_{\rm total} = \chi^2_{\rm GRB} + \chi^2_{\rm OHD}. \tag{5}$$

We perform MCMC fitting to constrain the DE models. Constraints using 140 GRBs at $z > 1.4$ are shown in Figures 4 (for the ΛCDM model) and 5 (for the CPL model); and joint constraints using 140 GRBs at $z > 1.4$ and 32 OHD are presented in Figures 6 (for ΛCDM model) and 7 (for CPL model), which are summarized in Table 3. We find that the inclusion of OHD in the joint constraints can tighten the constraints significantly. The results for the CPL model at the 1σ confidence level favor a possible DE evolution ($w_a \neq 0$). We find that the ANN+BNN results are consistent with those obtained by GaPP, while showing slight differences. Compared to the fitting results from CMB data based on the ΛCDM model at very high redshift (H_0 = 67.36 km s^{-1} Mpc^{-1}, Ω_m = 0.315) [110] and SNe Ia at very low redshift (H_0 = 74.3 km s^{-1} Mpc^{-1}, Ω_m = 0.298) [67], we find that the H_0 value with GRBs at $1.4 \leq z \leq 8.2$ and OHD at $z \leq 1.975$ favors the one from the Planck observations and that the Ω_m value of our results for the flat ΛCDM model is consistent with the CMB observations at the 1σ confidence level.

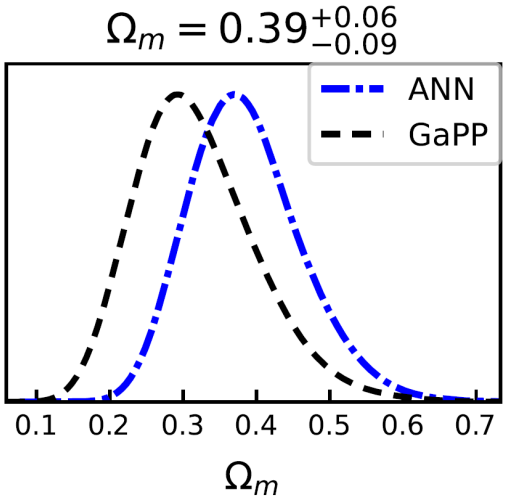

Figure 4. Constraints on Ω_m for the flat ΛCDM model using 140 GRBs ($z > 1.4$) by ANN and GaPP methods, with H_0 fixed at 70 km/s/Mpc.

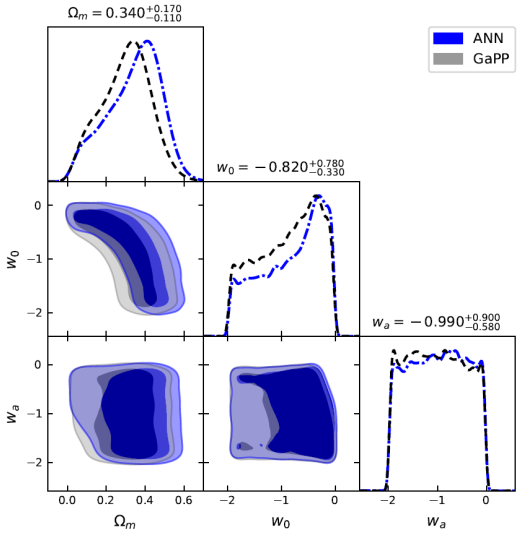

Figure 5. Constraints on Ω_m, w_0, and w_a for the flat CPL model using 140 GRBs ($z > 1.4$) by ANN and GaPP methods, with H_0 fixed at 70 km/s/Mpc.

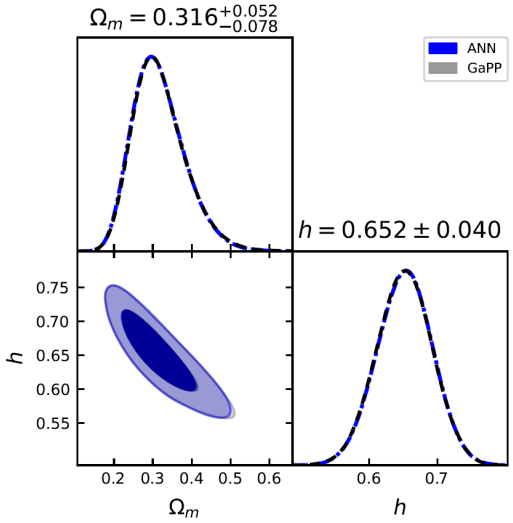

Figure 6. Joint constraints on Ω_m and h for the flat ΛCDM model using 140 GRBs ($z > 1.4$) + 32 OHD by the ANN and GaPP methods.

Table 3. Constraints on cosmological parameters for flat ΛCDM and CPL models by the ANN and GaPP methods with GRBs ($z > 1.4$) only and GRBs ($z > 1.4$) + OHD.

Models	Method	Data Sets	Ω_m	h	w_0	w_a	$-2\ln\mathcal{L}$	ΔAIC	ΔBIC
ΛCDM	ANN	140 GRBs	$0.385^{+0.062}_{-0.087}$	-	-	-	53.059	-	-
	GaPP	140 GRBs	$0.318^{+0.064}_{-0.096}$	-	-	-	40.402	-	-
	ANN	140 GRBs + 32 OHD	$0.316^{+0.052}_{-0.078}$	$0.652^{+0.040}_{-0.040}$	-	-	78.576	-	-
	GaPP	140 GRBs + 32 OHD	$0.318^{+0.051}_{-0.078}$	$0.652^{+0.040}_{-0.040}$	-	-	80.785	-	-
CPL	ANN	140 GRBs	$0.340^{+0.170}_{-0.110}$	-	$-0.82^{+0.78}_{-0.33}$	$-0.99^{+0.90}_{-0.58}$	53.158	3.901	9.784
	GaPP	140 GRBs	$0.300^{+0.150}_{-0.110}$	-	$-0.88^{+0.82}_{-0.33}$	$-1.01^{+0.52}_{-0.91}$	40.407	3.995	9.879
	ANN	140 GRBs + 32 OHD	$0.317^{+0.082}_{-0.072}$	$0.652^{+0.053}_{-0.072}$	$-0.99^{+0.71}_{-0.45}$	$-0.96^{+0.58}_{-0.58}$	78.953	3.622	9.917
	GaPP	140 GRBs + 32 OHD	$0.314^{+0.086}_{-0.068}$	$0.652^{+0.051}_{-0.072}$	$-0.99^{+0.72}_{-0.45}$	$-0.95^{+0.57}_{-0.57}$	81.227	3.554	9.848

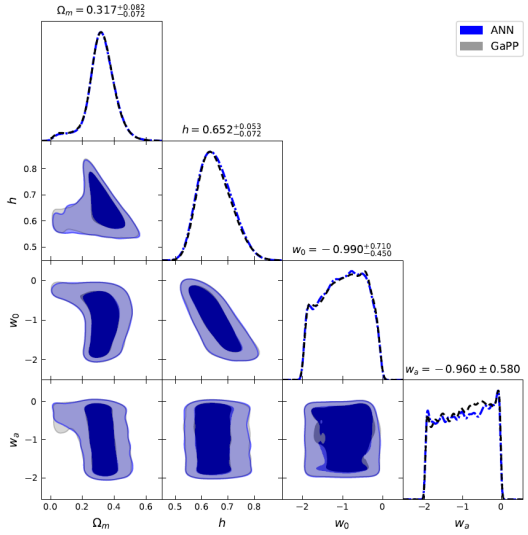

Figure 7. Joint constraints on Ω_m, h, w_0, and w_a for the flat CPL model using 140 GRBs ($z > 1.4$) + 32 OHD by the ANN and GaPP methods.

We also compare models using the Akaike Information Criterion (AIC) and Bayesian Information Criterion (BIC). The values of ΔAIC and ΔBIC relative to the reference model (the ΛCDM model) are given by: $\Delta\mathrm{AIC} = \Delta\chi^2_{\min} + 2\Delta k$, $\Delta\mathrm{BIC} = \Delta\chi^2_{\min} + \Delta k \ln N$. We find that the results of ΔAIC and ΔBIC indicate that the ΛCDM model is favoured respect to the CPL model.

5. Conclusions

In this paper, we use an ANN+BNN to calibrate the Amati relation from the Pantheon+ sample to obtain the GRB Hubble diagram with the A219 sample in a cosmology−independent way. Using the ANN method with GRBs at $0.8 < z < 8.2$ in the A219 sample and 32 OHD, we find that the results for the CPL model favor a possible DE evolution ($w_a \neq 0$) at the $1-\sigma$ confidence region. Compared to GP, which imposes strict Gaussian assumptions, ANN eliminates distributional constraints, enabling robust analysis of non−Gaussian observational datasets. Our results with GRBs at $1.4 \leq z \leq 8.2$ are consistent with previous analyses in [40,55,94] using GP methods.

We find that the calibration results of the slope in the Amati relation provided by Reichart method are close to the typical value ($b = 2$). The physical interpretation of the Amati relation can be provided by a model for the spectral formation of GRB prompt emission [111]. If the timescale of the GRB prompt emission and its shape for any burst is more or less the same, then E_p proportional to $E_{\rm iso}^{1/2}$ is seen precisely. Frontera et al. [112] have concluded that the Yonetoku relation (the spectral peak energy E_p to the isotropic

bolometric luminosity $L_{\rm iso}$) is intrinsic to the emission process, and their results strongly support the reality of both the Amati and Yonetoku relations derived using time-averaged spectra.

Recently,Ref.[59] presented a sample of long GRBs from fifteen years of the Fermi−GBM catalogue with identified redshift, in which the GOLD sample contains 123 long GRBs at $z \leq 5.6$ and the FULL sample contains 151 long GRBs with redshifts at $z \leq 8.2$. In [113], the authors analyzed 151 Fermi−observed long GRBs to simultaneously constrain the Amati correlation and cosmological parameters within six spatially flat and non−flat dark energy models. We expect that GRBs could be used to set tighter constraints on cosmological models by using the ANN approach with samples from recent Fermi data [59].

Author Contributions: Conceptualization, Z.H. and N.L.; methodology, B.Z.; software, X.L.; validation, Z.H., L.X. and B.Z.; formal analysis, B.Z.; data curation, Z.H., X.L. and B.Z.; writing—original draft preparation, Z.H. , B.Z. and N.L.; writing—review and editing, J.F., Y.L., P.W. and N.L.; supervision, N.L.; project administration, N.L.; funding acquisition, J.F., Y.L., P.W. and N.L. All authors have read and agreed to the published version of the manuscript.

Funding: This project was supported by the Guizhou Provincial Science and Technology Foundations (QKHJC−ZK[2021] Key 020, QKHJC−ZK[2024] General 443 and QKHPT ZSYS [2025] 004). Y. Liu was supported by the NSFC under Grant No. 12373063. P. Wu was supported by the National Natural Science Foundation of China (Grants No. 12275080) and the Innovative Research Group of Hunan Province (Grant No. 2024JJ1006). J. Feng was supported by the Guizhou Provincial Science and Technology Foundations QKHJC−ZK[2022] General 311.

Data Availability Statement: Data are contained within the article.

Acknowledgments: We thank the anonymous referees for their helpful comments and constructive suggestions.

Conflicts of Interest: The authors declare no conflicts of interest.

Notes

1 The 2D Dainotti relation [78] is the correlation between the plateau luminosity and its end time in X−ray afterglows; the 3D Dainotti relation [79] is the correlation incorporating the peak prompt luminosity with the plateau end time and luminosity in the rest frame, achieving a small intrinsic scatter.

2 We incorporate the Pantheon+ covariance matrix $C_{\rm SN}$ into the loss function: $\mathcal{L}_{\rm SN} = \Delta m(z_i)^T C_{\rm SN}^{-1} \Delta m(z_i)$, where $\Delta m(z_i) = m(z_i)_{\rm pred} - m(z_i)_{\rm obs}$ represents the difference between predicted and observed magnitudes.

3 The A219 sample is refined from the A220 sample [32] by removing the GRB051109A.

4 The distance module of SN Ia is related to the luminosity distance and the absolute magnitude (M); the value of M cannot be directly obtained using only the SN Ia sample, and as such M is treated as a free parameter.

5 Likelihood method of [92]: $\mathcal{L}_{\rm R} \propto \prod_{i=1}^{N_1} \frac{\sqrt{1+b^2}}{\sigma} \times \exp\left[-\frac{[y_i' - y'(x_i,z_i;a',b)]^2}{2\sigma^2}\right]$, where $\sigma = \sqrt{\sigma_{\rm int}^2 + \sigma_{y',i}^2 + b^2\sigma_{x,i}^2}$ and the intrinsic scatter is $\sigma_{\rm int} = \sqrt{\sigma_{y',\rm int}^2 + b^2\sigma_{x,\rm int}^2}$.

6 The uncertainty in the apparent magnitude is calculated as follows: $\sigma_m^2 = \left(\frac{5}{2}\sigma_{y'}(a',b,x,\sigma_{\rm int})\right)^2 + \left(\frac{5}{2\ln 10}\frac{\sigma_{S_{\rm bolo}}}{S_{\rm bolo}}\right)^2$, where: $\sigma_{y'}^2(a',b,\sigma_{\rm int},x) = \sigma_{\rm int}^2 + \left(\frac{b}{\ln 10}\frac{\sigma_{E_{\rm P}}}{E_{\rm P}}\right)^2 + \sigma_{y'}^2(a',b)$ and $\sigma_{y'}^2(a',b) = \left(\frac{\partial y'}{\partial a'}\right)^2\sigma_{a'}^2 + \left(\frac{\partial y'}{\partial b}\right)^2\sigma_b^2 + 2\left(\frac{\partial y'}{\partial a'}\right)\left(\frac{\partial y'}{\partial b}\right)C_{a'b}^{-1}$, with $(C^{-1})_{a'b} = \frac{\partial^2 L}{\partial a' \partial b}$.

7 The luminosity distance in a flat universe is expressed as $d_{L;\rm th} = \frac{c(1+z)}{H_0}\int_0^z \frac{dz'}{E(z')}$, where $E(z) = [\Omega_{\rm m}(1+z)^3 + \Omega_{\rm DE}(1+z)^{3(1+w_0+w_a)}e^{-\frac{3w_a z}{1+z}}]^{1/2}$, $\Omega_{\rm m}$ and $\Omega_{\rm DE}$ are respectively the matter and DE density parameters, with $\Omega_{\rm m} + \Omega_{\rm DE} = 1$ for flat geometry. For the ΛCDM model, $w_0 = -1$ and $w_a = 0$.

8 An alternative OHD point at $z = 0.75$ is available [108], but due to unclear covariance with [107], we use only the latter, which accounts for a $1/\sqrt{2}$ fraction of systematic uncertainty.

References

1. Dai, Z.; Liang, E.; Xu, D. Constraining Ω_M and Dark Energy with Gamma-Ray Bursts. *Astrophys. J.* **2004**, *612*, L101. https://doi.org/10.1086/424694.
2. Firmani, C.; Ghisellini, G.; Ghirlanda, G.; Avila-Reese, V. A new method optimized to use gamma-ray bursts as cosmic rulers. *Mon. Not. R. Astron. Soc.* **2005**, *360*, L1. https://doi.org/10.1111/j.1745-3933.2005.00023.x.
3. Ghirlanda, G.; Ghisellini, G.; Lazzati, D.; Firmani, C. Gamma-Ray Bursts: New Rulers to Measure the Universe. *Astrophys. J.* **2004**, *613*, L13. https://doi.org/10.1086/424915.
4. Ghirlanda, G.; Ghisellini, G.; Firmani, C. Gamma-ray bursts as standard candles to constrain the cosmological parameters. *New J. Phys.* **2006**, *8*, 123. https://doi.org/10.1088/1367-2630/8/7/123.
5. Liang, E.; Zhang, B. Calibration of gamma-ray burst luminosity indicators. *Mon. Not. R. Astron. Soc.* **2006**, *369*, L37. https://doi.org/10.1111/j.1745-3933.2006.00169.x.
6. Schaefer, B.E. Gamma-Ray Burst Hubble Diagram to z = 4.5. *Astrophys. J.* **2003**, *583*, L67. https://doi.org/10.1086/368104.
7. Schaefer, B.E. The Hubble Diagram to Redshift >6 from 69 Gamma-Ray Bursts. *Astrophys. J.* **2007**, *660*, 16. https://doi.org/10.1086/511742.

8. Wang, F.; Dai, Z.G. Constraining the cosmological parameters and transition redshift with gamma-ray bursts and supernovae. *Mon. Not. R. Astron. Soc.* **2006**, *368*, 371. https://doi.org/10.1111/j.1365-2966.2006.10108.x.
9. Xu, D.; Dai, Z.; Liang, E. Can Gamma-Ray Bursts Be Used to Measure Cosmology? A Further Analysis. *Astrophys. J.* **2005**, *633*, 603. https://doi.org/10.1086/466509.
10. Liang, N.; Xiao, W.K.; Liu, Y.; Zhang, S.N. A Cosmology-Independent Calibration of Gamma-Ray Burst Luminosity Relations and the Hubble Diagram. *Astrophys. J.* **2008**, *685*, 354. https://doi.org/10.1086/590903.
11. Amati, L.; D'Agostino, R.; Luongo, O.; Muccino, M.; Tantalo, M. Addressing the circularity problem in the E_p-E_{iso} correlation of gamma-ray bursts. *Mon. Not. R. Astron. Soc.* **2019**, *486*, L46. https://doi.org/10.1093/mnrasl/slz056.
12. Amati, L.; Frontera, F.; Tavani, M.; in't Zand, J.J.M.; Antonelli, A.; Costa, E.; Feroci, M.; Guidorzi, C.; Heise, J.; Masetti, N.; et al. Intrinsic spectra and energetics of BeppoSAX Gamma-Ray Bursts with known redshifts. *Astron. Astrophys.* **2002**, *390*, 81. https://doi.org/10.1051/0004-6361:20020722.
13. Capozziello, S.; Izzo, L. Cosmography by gamma ray bursts. *Astron. Astrophys.* **2008**, *490*, 31. https://doi.org/10.1051/0004-6361:200810337.
14. Capozziello, S.; Izzo, L. Cosmography by GRBs: Gamma Ray Bursts as possible distance indicators. *Nucl. Phys. B Proc. Suppl.* **2009**, *194*, 206. https://doi.org/10.1016/j.nuclphysbps.2009.07.024.
15. Demianski, M.; Piedipalumbo, E.; Sawant, D.; Amati, L. Cosmology with gamma-ray bursts. I. The Hubble diagram through the calibrated $E_{p,I}$-E_{iso} correlation. *Astron. Astrophys.* **2017**, *598*, A112. https://doi.org/10.1051/0004-6361/201628909.
16. Demianski, M.; Piedipalumbo, E.; Sawant, D.; Amati, L. Cosmology with gamma-ray bursts. II. Cosmography challenges and cosmological scenarios for the accelerated Universe. *Astron. Astrophys.* **2017**, *598*, A113. https://doi.org/10.1051/0004-6361/201628911.
17. Liang, N.; Wu, P.; ; Zhang, S.N. Constraints on cosmological models and reconstructing the acceleration history of the Universe with gamma-ray burst distance indicators. *Phys. Rev. D* **2010**, *81*, 083518. https://doi.org/10.1103/PhysRevD.81.083518.
18. Liang, N.; Xu, L.; ; Zhu, Z.H. Constraints on the generalized Chaplygin gas model including gamma-ray bursts via a Markov Chain Monte Carlo approach. *Astron. Astrophys.* **2011**, *527*, A11. https://doi.org/10.1051/0004-6361/201015919.
19. Wei, H.; Zhang, S.N. Reconstructing the cosmic expansion history up to redshift z = 6.29 with the calibrated gamma-ray bursts. *Eur. Phys. J. C* **2009**, *63*, 139. https://doi.org/10.1140/epjc/s10052-009-1086-z.
20. Wei, H. Observational constraints on cosmological models with the updated long gamma-ray bursts. *J. Cosmol. Astropart. Phys.* **2010**, *8*, 020. https://doi.org/10.1088/1475-7516/2010/08/020.
21. Luongo, O.; Muccino, M. Intermediate redshift calibration of gamma-ray bursts and cosmic constraints in non-flat cosmology. *Mon. Not. R. Astron. Soc.* **2023**, *518*, 2247. https://doi.org/10.1093/mnras/stac2925.
22. Montiel, A.; Cabrera, J.I.; ; Hidalgo, J.C. Improving sampling and calibration of gamma-ray bursts as distance indicators. *Mon. Not. R. Astron. Soc.* **2021**, *467*, 3239. https://doi.org/10.1093/mnras/staa3926.
23. Wang, J.S.; Wang, F.Y.; Cheng, K.S.; Dai, Z.G. Measuring dark energy with the E_{iso} - E_p correlation of gamma-ray bursts using model-independent methods. *Astron. Astrophys.* **2016**, *585*, A68. https://doi.org/10.1051/0004-6361/201526485.
24. Wang, Y.Y.; Wang, F.Y. Calibration of Gamma-Ray Burst Luminosity Correlations Using Gravitational Waves as Standard Sirens. *Astrophys. J.* **2019**, *873*, 39. https://doi.org/10.3847/1538-4357/ab037b.
25. Dai, Y.; Zheng, X.-G.; Li, Z.-X.; Gao, H.; Zhu, Z.-H. Redshift evolution of the Amati relation: Calibrated results from the Hubble diagram of quasars at high redshifts. *Astron. Astrophys.* **2021**, *651*, L8. https://doi.org/10.1051/0004-6361/202140895.
26. Purohit, S.; Desai, S. Calibration of Luminosity Correlations of Gamma-Ray Bursts Using Quasars. *Galaxies* **2024**, *12*, 69. https://doi.org/10.3390/galaxies12060069.
27. Gowri, G.; Shantanu, D. Low redshift calibration of the Amati relation using galaxy clusters. *J. Cosmol. Astropart. Phys.* **2022**, *10*, 069. https://doi.org/10.1088/1475-7516/2022/10/069.
28. Amati, L.; Guidorzi, C.; Frontera, F.; Della Valle, M.; Finelli, F.; Landi, F.; Montanari, E. Measuring the cosmological parameters with the $E_{p,i}$-E_{iso} correlation of gamma-ray bursts. *Mon. Not. R. Astron. Soc.* **2008**, *391*, 577. https://doi.org/10.1111/j.1365-2966.2008.13943.x.
29. Cao, S.; Dainotti, M.; Ratra, B. Standardizing Platinum Dainotti-correlated gamma-ray bursts, and using them with standardized Amati-correlated gamma-ray bursts to constrain cosmological model parameters. *Mon. Not. R. Astron. Soc.* **2022**, *512*, 439. https://doi.org/10.1093/mnras/stac517.
30. Cao, S.; Khadka, N.; Ratra, B. Standardizing Dainotti-correlated gamma-ray bursts, and using them with standardized Amati-correlated gamma-ray bursts to constrain cosmological model parameters. *Mon. Not. R. Astron. Soc.* **2022**, *510*, 2928. https://doi.org/10.1093/mnras/stab3559.
31. Khadka, N.; Ratra, B. Constraints on cosmological parameters from gamma-ray burst peak photon energy and bolometric fluence measurements and other data. *Mon. Not. R. Astron. Soc.* **2020**, *499*, 391. https://doi.org/10.1093/mnras/staa2779.
32. Khadka, N.; Luongo, O.; Muccino, M.; Ratra, B. Do gamma-ray burst measurements provide a useful test of cosmological models? *J. Cosmol. Astropart. Phys.* **2021**, *09*, 042. https://doi.org/10.1088/1475-7516/2021/09/042.

33. Cao, S.; Ratra, B. Using lower redshift, non-CMB, data to constrain the Hubble constant and other cosmological parameters. *Mon. Not. R. Astron. Soc.* **2022**, *513*, 5686. https://doi.org/10.1093/mnras/stac1184.
34. Colgáin, E.O.; Sheikh-Jabbari, M.M.; Yin, L. Do high redshift QSOs and GRBs corroborate JWST? *Phys. Dark Universe* **2025**, *49*, 101975. https://doi.org/10.1016/j.dark.2025.101975.
35. Favale, A.; Dainotti, M.G.; Gómez-Valent, A.; Migliaccio, M. Towards a new model-independent calibration of Gamma-Ray Bursts. *J. High Energy Astrophys.* **2024**, *44*, 323. https://doi.org/10.1016/j.jheap.2024.10.010.
36. Han, Y.; Gao, J.; Liu, G.; Xu, L. Detection of gamma-ray burst Amati relation based on Hubble data set and Pantheon+ samples. *Eur. Phys. J. C* **2024**, *84*, 934. https://doi.org/10.1140/epjc/s10052-024-13304-5.
37. Hu, J.P.; Wang, F.Y.; Dai, Z.G. Measuring cosmological parameters with a luminosity-time correlation of gamma-ray bursts. *Mon. Not. R. Astron. Soc.* **2021**, *507*, 730. https://doi.org/10.1093/mnras/stab2180.
38. Li, J.-L.; Yang, Y.-P.; Yi, S.-X.; Hu, J.-P.; Qu, Y.-K.; Wang, F.-Y. Standardizing the gamma-ray burst as a standard candle and applying it to cosmological probes: Constraints on the two-component dark energy model. *Astron. Astrophys.* **2024**, *689*, A165. https://doi.org/10.1051/0004-6361/202348542.
39. Liu, Y.; Chen, F.; Liang, N.; Yuan, Z.; Yu, H.; Wu, P. The Improved Amati Correlations from Gaussian Copula. *Astrophys. J.* **2022**, *931*, 50. https://doi.org/10.3847/1538-4357/ac66d3.
40. Liu, Y.; Liang, N.; Xie, X.; Yuan, Z.; Yu, H.; Wu, P. Gamma-Ray Burst Constraints on Cosmological Models from the Improved Amati Correlation. *Astrophys. J.* **2022**, *935*, 7. https://doi.org/10.3847/1538-4357/ac7de5.
41. Paliathanasis, A. Testing Non-Coincident $f(Q)$-gravity with DESI DR2 BAO and GRBs. *arXiv* **2025**, arXiv:2504.11132. https://doi.org/10.48550/arXiv.2504.11132.
42. Tian, X.; Li, J.-L.; Yi, S.-X.; Yang, Y.-P.; Hu, J.-P.; Qu, Y.-K.; Wang, F.-Y. Radio Plateaus in Gamma-Ray Burst Afterglows and Their Application in Cosmology. *Astrophys. J.* **2023**, *958*, 74. https://doi.org/10.3847/1538-4357/acfed8.
43. Bargiacchi, G.; Dainotti, M.G.; Hernandez, X. High-redshift cosmology by Gamma-Ray Bursts: An overview. *New Astron. Rev.* **2025**, *100*, 101712. https://doi.org/10.1016/j.newar.2024.101712.
44. Deng, C.; Huang, Y.-F.; Xu, F.; Kurban, A. The Observed Luminosity Correlations of Gamma-Ray Bursts and Their Applications. *Galaxies* **2025**, *13*, 15. https://doi.org/10.3390/galaxies13020015.
45. Liang, N.; Zhang, S. Cosmology-Independent Distance Moduli of 42 Gamma-Ray Bursts between Redshift of 1.44 and 6.60. *AIP Conf. Proc.* **2008**, *1065*, 367–372. https://doi.org/10.1063/1.3027949.
46. Kodama, Y.; Yonetoku, D.; Murakami, T.; Tanabe, S.; Tsutsui, R.; Nakamura, T. Gamma-ray bursts in 1.8 < z < 5.6 suggest that the time variation of the dark energy is small. *Mon. Not. R. Astron. Soc.* **2008**, *391*, L1. https://doi.org/10.1111/j.1745-3933.2008.00508.x.
47. Cardone, V.F.; Capozziello, S.; Dainotti, M.G. An updated gamma-ray bursts Hubble diagram. *Mon. Not. R. Astron. Soc.* **2009**, *400*, 775. https://doi.org/10.1111/j.1365-2966.2009.15456.x.
48. Capozziello, S.; Izzo, L. A cosmographic calibration of the $E_{p,i}$ - E_{iso} (Amati) relation for GRBs. *Astron. Astrophys.* **2010**, *519*, A73. https://doi.org/10.1051/0004-6361/201014522.
49. Gao, H.; Liang, N.; Zhu, Z.-H. Calibration of GRB Luminosity Relations with Cosmography. *Int. J. Mod. Phys. D* **2012**, *21*, 1250016. https://doi.org/10.1142/S0218271812500162.
50. Liu, J.; Wei, H. Cosmological models and gamma-ray bursts calibrated by using Padé method. *Gen. Relativ. Gravit.* **2015**, *47*, 141. .
51. Izzo, L.; Muccino, M.; Zaninoni, E.; Amati, L.; Della Valle, M. New measurements of Ω_m from gamma-ray bursts. *Astron. Astrophys.* **2015**, *582*, A115. https://doi.org/10.1051/0004-6361/201526461.
52. Muccino, M.; Izzo, L.; Luongo, O.; Boshkayev, K.; Amati, L.; Della Valle, M.; Pisani, G. B.; Zaninoni, E. Tracing Dark Energy History with Gamma-Ray Bursts. *Astrophys. J.* **2021**, *908*, 181. https://doi.org/10.3847/1538-4357/abd254.
53. Seikel, M.; Clarkson, C.; Smith, M. Reconstruction of dark energy and expansion dynamics using Gaussian processes. *J. Cosmol. Astropart. Phys.* **2012**, *6*, 036. https://doi.org/10.1088/1475-7516/2012/06/036.
54. Li, J.-L.; Yang, Y.-P.; Yi, S.-X.; Hu, J.-P.; Wang, F.-Y.; Qu, Y.-K. Constraints on the Cosmological Parameters with Three-Parameter Correlation of Gamma-Ray Bursts. *Astrophys. J.* **2023**, *953*, 58. https://doi.org/10.3847/1538-4357/ace107.
55. Liang, N.; Li, Z.; Xie, X.; Wu, P. Calibrating Gamma-Ray Bursts by Using a Gaussian Process with Type Ia Supernovae. *Astrophys. J.* **2022**, *941*, 84. https://doi.org/10.3847/1538-4357/aca08a.
56. Mu, Y.; Chang, B.; Xu, L. Cosmography via Gaussian process with gamma ray bursts. *J. Cosmol. Astropart. Phys.* **2023**, *9*, 041. https://doi.org/10.1088/1475-7516/2023/09/041.
57. Nong, X.-D.; Liang, N. Testing the Phenomenological Interacting Dark Energy Model with Gamma-Ray Bursts and Pantheon+ type Ia Supernovae. *Res. Astron. Astrophys.* **2024**, *24*, 125003. https://doi.org/10.1088/1674-4527/ad8a07.
58. Wang, G.Z.; ; Li, X.L.; Liang, N. Constraining the emergent dark energy models with observational data at intermediate redshift. *Astrophys. Space Sci.* **2024**, *369*, 74. https://doi.org/10.1007/s10509-024-04340-4.
59. Wang, H.; Liang, N. Constraints from Fermi observations of long gamma-ray bursts on cosmological parameters. *Mon. Not. R. Astron. Soc.* **2024**, *533*, 743. https://doi.org/10.1093/mnras/stae1825.

60. Xie, H.; Nong, X.; Wang, H.; Zhang, B.; Li, Z.; Liang, N. Constraints on cosmological models with gamma-ray bursts in cosmology-independent way. *Int. J. Mod. Phys. D* **2025**, *20*, 2450073. https://doi.org/10.1142/S0218271824500731.
61. Seikel, M.; Yahya, S.; Maartens, R.; ; Clarkson, C. Using H(z) data as a probe of the concordance model. *Phys. Rev. D* **2012**, *86*, 083001. https://doi.org/10.1103/PhysRevD.86.083001.
62. Wei, J.-J.; Wu, X.-F. An Improved Method to Measure the Cosmic Curvature. *Astrophys. J.* **2017**, *838*, 160w. https://doi.org/10.3847/1538-4357/aa674b.
63. Zhou, H.; Li, Z. Testing the fidelity of Gaussian processes for cosmography. *Chin. Phys.* **2019**, *43*, 035103. https://doi.org/10.1088/1674-1137/43/3/035103.
64. Luongo, O.; Muccino, M. Model-independent calibrations of gamma-ray bursts using machine learning. *Mon. Not. R. Astron. Soc.* **2021**, *503*, 4581. https://doi.org/10.1093/mnras/stab795.
65. Bengaly, C.; Dantas, ; M.A.; ; Casarini, L.; Alcaniz, J. Measuring the Hubble constant with cosmic chronometers: A machine learning approach. *Eur. Phys. J.* **2023**, *83*, 548. https://doi.org/10.1140/epjc/s10052-023-11734-1.
66. Zhang, B.; Wang, H.; Nong, X.; Wang, G.; Wu, P.; Liang, N. Model-independent gamma-ray bursts constraints on cosmological models using machine learning. *Astrophys. Space Sci.* **2025**, *370*, 10. https://doi.org/10.1007/s10509-025-04401-2
67. Scolnic, D.; Brout, D.; Carr, A.; Riess, A.G.; Davis, T.M.; Dwomoh, A.; Jones, D.O.; Ali, N.; Charvu, P.; Chen, R.; et al. The Pantheon+ Analysis: The Full Data Set and Light-curve Release. *Astrophys. J.* **2022**, *938*, 113. https://doi.org/10.3847/1538-4357/ac8b7a.
68. Chen, J.F.; Zhang, T.J.; He, P.; Zhang, T.; Zhang, J. Estimating Cosmological Parameters and Reconstructing Hubble Constant with Artificial Neural Networks: A Test with covariance matrix and mock H(z). *arXiv* **2024**, arXiv:2410.08369. https://doi.org/10.48550/arXiv.2410.08369.
69. Dialektopoulos, K.; Said, J.L.; Mifsud, J.; Sultana, J.; Adami, K.Z. Neural network reconstruction of late-time cosmology and null tests. *J. Cosmol. Astropart. Phys.* **2022**, *2*, 023. https://doi.org/10.1088/1475-7516/2022/02/023.
70. Di Valentino, E.; Levi Said, J.; Riess, A.; Pollo, A.; Poulin, V.; Gómez-Valent, A.; Weltman, A.; Palmese, A.; Huang, C.; van de Bruck, C.; et al. The CosmoVerse White Paper: Addressing observational tensions in cosmology with systematics and fundamental physics. *arXiv* **2025**, arXiv.2405.19953. https://doi.org/10.48550/arXiv.2504.01669.
71. Escamilla-Rivera, C.; Quintero, M.A.C.; Capozziello, S. A deep learning approach to cosmological dark energy models. *J. Cosmol. Astropart. Phys.* **2020**, *3*, 008. https://doi.org/10.1088/1475-7516/2020/03/008.
72. Gómez-Vargas, I.; Medel-Esquivel, R.; García-Salcedo, R.; Vázquez, J.A. Neural network reconstructions for the Hubble parameter, growth rate and distance modulus. *Eur. Phys. J. C* **2023**, *83*, 304. https://doi.org/10.1140/epjc/s10052-023-11435-9.
73. Niu, J.; He, P.; Zhang, T.-J. Constraining the Hubble Constant with a Simulated Full Covariance Matrix Using Neural Networks. *arXiv* **2025**, arXiv:2502.11443. https://doi.org/10.48550/arXiv.2502.11443.
74. Wang, G.-J.; Ma, X.-J.; Li, S.-Y.; Xia, J.-Q. Reconstructing Functions and Estimating Parameters with Artificial Neural Networks: A Test with a Hubble Parameter and SNe Ia. *Astrophys. J. Suppl. Ser.* **2020**, *246*, 13. https://doi.org/10.3847/1538-4365/ab620b.
75. Zhang, J.C.; Hu, Y.; Jiao, K.; Wang, H.F.; Xie, Y.B.; Yu, B.; Zhao, L.L.; Zhang, T.J. A Nonparametric Reconstruction of the Hubble Parameter H(z) Based on Radial Basis Function Neural Networks. *Astrophys. J. Suppl. Ser.* **2024**, *270*, 23. https://doi.org/10.3847/1538-4365/ad0f1e.
76. Shah, R.; Saha, S.; Mukherjee, P.; Garain, U.; Pal, S. LADDER: Revisiting the Cosmic Distance Ladder with Deep Learning Approaches and Exploring Its Applications. *Astrophys. J. Suppl. Ser.* **2024**, *273*, 27. https://doi.org/10.3847/1538-4365/ad5558.
77. Mukherjee, P.; Dainotti, M.; Dialektopoulos, K.F.; Levi, Said, J.; Mifsud, J. Model-independent calibration of Gamma-Ray Bursts with neural networks. *arXiv* **2024**, arXiv:2411.03773. https://doi.org/10.48550/arXiv.2411.03773.
78. Dainotti, M.G.; Cardone, V.F.; Capozziello, S. A time-luminosity correlation for γ-ray bursts in the X-rays. *Mon. Not. R. Astron. Soc.* **2008**, *391*, L79. https://doi.org/10.1111/j.1745-3933.2008.00560.x .
79. Dainotti, M.G.; Postnikov, S.; Hernandez, X.; Ostrowski M. A Fundamental Plane for Long Gamma-Ray Bursts with X-Ray Plateaus. *Astrophys. J.* **2016**, *825*, L20. https://doi.org/10.3847/2041-8205/825/2/L20.
80. Huang, Z.; Xiong, Z.; Luo, X.; Wang, G.; Liu, Y.; Liang, N. Gamma-ray bursts calibrated from the observational H(z) data in artificial neural network framework. *J. High Energy Astrophys.* **2025**, *47*, 100337. https://doi.org/10.1016/j.jheap.2025.100377.
81. Cao, S.; Ratra, B. Testing the standardizability of, and deriving cosmological constraints from, a new Amati-correlated gamma-ray burst data compilation. *J. Cosmol. Astropart. Phys.* **2024**, *10*, 093. https://doi.org/10.1088/1475-7516/2024/10/093.
82. Jia, X.D.; Hu, J.P.; Yang, J.; Zhang, B.B.; Wang, F.Y. E_{iso}-E_p correlation of gamma-ray bursts: Calibration and cosmological applications. *Mon. Not. R. Astron. Soc.* **2022**, *516*, 2575. https://doi.org/10.1093/mnras/stac2356.
83. Escamilla-Rivera, C.; Carvajal, M.; Zamora, C.; Hendry, M. Neural networks and standard cosmography with newly calibrated high redshift GRB observations. *J. Cosmol. Astropart. Phys.* **2022**, *4*, 016. https://doi.org/10.1088/1475-7516/2022/04/016.
84. Tang, L.; Li, X.; Lin, H.-N.; Liu, L. Model-independently Calibrating the Luminosity Correlations of Gamma-Ray Bursts Using Deep Learning. *Astrophys. J.* **2021**, *907*, 121. https://doi.org/10.3847/1538-4357/abcd92.
85. Tang, L.; Lin, H.-N.; Li, X.; Liu, L. Reconstructing the Hubble diagram of gamma-ray bursts using deep learning. *Mon. Not. R. Astron. Soc.* **2022**, *509*, 1194. https://doi.org/10.1093/mnras/stab2932.

86. Rumelhart, D.E.; Hinton, G.E.; Williams, R.J. Learning representations by back-propagating errors. *Nature* **1986**, *323*, 533. https://doi.org/10.1038/323533a0.
87. Gal, Y.; Ghahramani, Z. Dropout as a Bayesian Approximation: Representing Model Uncertainty in Deep Learning. *arXiv* **2016**, arXiv:1506.02142. https://doi.org/10.48550/arXiv.1506.02142.
88. Gal, Y.; Ghahramani, Z. Dropout as a Bayesian Approximation: Appendix. *arXiv* **2016**, arXiv:1506.02157. https://doi.org/10.48550/arXiv.1506.02157.
89. Srivastava, N.; Hinton, G.; Krizhevsky, A.; Sutskever, I.; Salakhutdinov, R. Dropout: A Simple Way to Prevent Neural Networks from Overftting. *J. Mach. Learn. Res.* **2014**, *15*, 1929. http://jmlr.org/papers/v15/srivastava14a.html.
90. Zhang, H.; Liu, Y.; Yu, H.; Nong, X.; Liang, N.; ; Wu, P. Constraints on cosmological models from quasars calibrated with type Ia supernova by a Gaussian process. *Mon. Not. R. Astron. Soc.* **2024**, *530*, 4493. https://doi.org/10.1093/mnras/stae1120. .
91. Foreman-Mackey, D.; Hogg, D.W.; Lang, D.; Goodman, J. emcee: The MCMC Hammer. *Publ. Astron. Soc. Pac.* **2013**, *125*, 306. https://doi.org/10.1086/670067.
92. Reichart, D.E. Dust Extinction Curves and Lyα Forest Flux Deficits for Use in Modeling Gamma-Ray Burst Afterglows and All Other Extragalactic Point Sources. *Astrophys. J.* **2001**, *553*, 57. https://doi.org/10.1086/320630.
93. Amati, L.; Della Valle, M. Measuring Cosmological Parameters with Gamma Ray Bursts. *Int. J. Mod. Phys.* **2013**, *22*, 1330028. https://doi.org/10.1142/S0218271813300280.
94. Li, Z.; Zhang, B.; ; Liang, N. Testing dark energy models with gamma-ray bursts calibrated from the observational H(z) data through a Gaussian process. *Mon. Not. R. Astron. Soc.* **2023**, *521*, 4406. https://doi.org/10.1093/mnras/stad838.
95. Demianski, M.; Piedipalumbo, E.; Sawant, D.; Amati, L. Prospects of high redshift constraints on dark energy models with the $E_{p,i}$-E_{iso} correlation in long gamma ray bursts. *Mon. Not. R. Astron. Soc.* **2021**, *506*, 903. https://doi.org/10.1093/mnras/stab1669.
96. Kumar, D.; Rani, N.; Jain, D.; Mahajan, S.; Mukherjee, A. Gamma rays bursts: A viable cosmological probe? *J. Cosmol. Astropart. Phys.* **2023**, *07*, 021. https://doi.org/10.1088/1475-7516/2023/07/021.
97. Lin, H.N.; Li, X.; Chang, Z. Model-independent distance calibration of high-redshift gamma-ray bursts and constrain on the ΛCDM model. *Mon. Not. R. Astron. Soc.* **2016**, *455*, 2131. https://doi.org/10.1093/mnras/stv2471.
98. Wang, G.-J.; Wei, J.-J.; Li, Z.-X.; Xia, J.-Q.; Zhu, Z.-H. Model-independent Constraints on Cosmic Curvature and Opacity. *Astrophys. J.* **2017**, *847*, 45. https://doi.org/10.3847/1538-4357/aa8725.
99. Chevallier, M.; Polarski, D. Accelerating Universes with Scaling Dark Matter. *Int. J. Mod. Phys. D* **2001**, *10*, 213. https://doi.org/10.1142/S0218271801000822.
100. Linder, E.V. Exploring the Expansion History of the Universe. *Phys. Rev. Lett.* **2003**, *90*, 091301.
101. Moresco, M.; Cimatti, A.; Jimenez, R.; Pozzetti, L.; Zamorani, G.; Bolzonella, M.; Dunlop, J.; Lamareille, F.; Mignoli, M.; Pearce, H.; et al. Improved constraints on the expansion rate of the Universe up to z $\sim$1.1 from the spectroscopic evolution of cosmic chronometers. *J. Cosmol. Astropart. Phys.* **2012**, *2012*, 006. https://doi.org/10.1088/1475-7516/2012/08/006.
102. Moresco, M. Raising the bar: New constraints on the Hubble parameter with cosmic chronometers at z $\sim$2. *Mon. Not. R. Astron. Soc.* **2015**, *450*, L16. https://doi.org/10.1093/mnrasl/slv037.
103. Moresco, M.; Pozzetti, L.; Cimatti, A.; Jimenez, R.; Maraston, C.; Verde, L.; Thomas, D.; ; Citro, A.; Tojeiro, R.; Wilkinson, D. A 6% measurement of the Hubble parameter at z$\sim$0.45: Direct evidence of the epoch of cosmic re-acceleration. *J. Cosmol. Astropart. Phys.* **2016**, *2016*, 014. https://doi.org/10.1088/1475-7516/2016/05/014.
104. Ratsimbazafy, A.L.; Loubser, S.I.; Crawford, S.M.; Cress, C.M.; Bassett, B.A.; Nichol, R.C.; Väisänen, P. Age-dating luminous red galaxies observed with the Southern African Large Telescope. *Mon. Not. R. Astron. Soc.* **2017**, *467*, 3239. https://doi.org/10.1093/mnras/stx301.
105. Stern, D.; Jimenez, R.; Verde, L.; Kamionkowski, M.; Starford, S.A. Cosmic chronometers: Constraining the equation of state of dark energy. I: H(z) measurements. *J. Cosmol. Astropart. Phys.* **2010**, *2010*, 008. https://doi.org/10.1088/1475-7516/2010/02/008.
106. Zhang, C.; Zhang, H.; Yuan, S.; Liu, S.; Zhang, T.; Sun, Y. Four new observational H(z) data from luminous red galaxies in the Sloan Digital Sky Survey data release seven. *Res. Astron. Astrophys.* **2014**, *14*, 1221. https://doi.org/10.1088/1674-4527/14/10/002.
107. Jiao, K.; Borghi, N.; Moresco, M.; Zhang, T.-J. New Observational H(z) Data from Full-spectrum Fitting of Cosmic Chronometers in the LEGA-C Survey. *Astrophys. J. Suppl. Ser.* **2023**, *265*, 48. https://doi.org/10.3847/1538-4365/acbc77.
108. Borghi, N.; Moresco, M.; Cimatti, A. Toward a Better Understanding of Cosmic Chronometers: A New Measurement of H(z) at z$\sim$0.7. *Astrophys. J.* **2022**, *928*, L4. https://doi.org/10.3847/2041-8213/ac3fb2.
109. Moresco, M.; Jimenez, R.; Verde, L.; Cimatti, A.; Pozzetti, L. Setting the Stage for Cosmic Chronometers. II. Impact of Stellar Population Synthesis Models Systematics and Full Covariance Matrix. *Astrophys. J.* **2020**, *898*, 82. https://doi.org/10.3847/1538-4357/ab9eb0.
110. Aghanim, N.; Akrami, Y.; Arroja, F.; Ashdown, M.; Aumont, J.; Baccigalupi, C.; Ballardini, M.; Banday, A.J.; Barreiro, R.B.; et al. Planck 2018 results. I. Overview and the cosmological legacy of Planck. *Astron. Astrophys.* **2020**, *641*, A1. https://doi.org/10.1051/0004-6361/201833880.

111. Titarchuk, L.; Farinelli, R.; Frontera, F.; Amati, L. An Upscattering Spectral Formation Model for the Prompt Emission of Gamma-Ray Bursts. *Astrophys. J.* **2012**, *752*, 116. https://doi.org/10.1088/0004-637X/752/2/116.
112. Frontera, F.; Amati, L.; Guidorzi, C.; Landi, R.; in't Zand, J. Broadband Time-resolved $E_{p,i}$-L_{iso} Correlation in Gamma-Ray Bursts. *Astrophys. J.* **2012**, *754*, 138. https://doi.org/10.1088/0004-637X/754/2/138.
113. Cao, S.; Ratra, B. Testing the consistency of new Amati-correlated gamma-ray burst dataset cosmological constraints with those from better-established cosmological data. *arXiv* **2025**, arXiv:2502.08429. https://doi.org/10.48550/arXiv.2502.08429.